# NUMERICAL SIMULATIONS OF A COMPACT TERAHERTZ SMITH-PURCELL FREE-ELECTRON LASER

C. R. Prokop[1]. P. Piot[1,2], M. C. Lin[3], P. Stoltz[3]
[1] Department of Physics, Northern Illinois University DeKalb, IL 60115, USA
[2] Accelerator Physics Center, Fermi National Accelerator Laboratory, Batavia, IL 60510, USA
[3] Tech-X Corporation, Boulder, CO 80303, USA

*Abstract*

Terahertz (THz) radiation occupies a very large portion of the electromagnetic spectrum and has generated much recent interest due to its ability to penetrate deep into many organic materials without the damage associated with ionizing radiation such as X-rays. One path for generating copious amount of tunable narrow-band THz radiation is based on the Smith-Purcell free-electron laser (SPFEL) effect first proposed by Wachtel [1]. In this paper we present the design and start-to-end simulation of a compact SPFEL. The device is based on a low energy ($< 100$ keV) electron accelerator capable of producing sheet electron beams needed to enhance the SPFEL interaction. The beam dynamics and electromagnetics of the SPFEL interaction are modeled using a finite-difference time-domain electromagnetic solver (VORPAL from Tech-X Corporation).

## INTRODUCTION

Over recent years, interest has grown in THz radiation over its ability to penetrate organic matter without ionizing damage (such as those from X-rays), making it ideal for biomedical scanning and homeland security purposes.

Unfortunately, the use and production of THz radiation has had significant drawbacks. Primarily, it occupies the same wavelength range as thermal background radiation, requiring intense sources and sensitive detectors. Current methods, such as impinging a laser on electro-optic crystals or photoconductive switches, are dependent on the energy of the laser pulse and provide broadband Terahertz radiation. Other methods based on free-electron lasers driven by MeV-energy electron beams are capable of providing narrow band tunable Terahertz radiation but are overly expensive.

In this paper, we concentrate on an alternative source of THz radiation based on a Smith-Purcell Free-Electron Laser (SPFEL) operating as a backward wave oscillator (BWO) [2, 3]. In such a device, a low energy electron beam is passed closed to a conducting grating. Doing so induces a back-propagating evanescent wave that can result in a beam density modulation provided the current density is large enough. The SPFEL process was first suggested and analyzed by Wachtel [1] and various theories have been developed over the past decades [2, 3, 4, 5], but attempts to produce the effect experimentally and validate its underlying theory have been inconclusive until very recently [6, 7].

One of our motivations for the work presented here is to explore, using an integrated model, the possibility of performing a proof-of-principle experiment to demonstrate the generation of THz radiation using a low energy DC gun available at Northern Illinois University [8].

## PARTICLE-IN-CELL SIMULATIONS OF THE SPFEL BWO PROCESS

The simulation of the SPFEL process is performed with VORPAL a conformal finite-difference time-domain (CFTDT) particle-in-cell (PIC) electromagnetic solver [9]. VORPAL is a parallel, object-oriented framework for three dimensional relativistic electrostatic and electromagnetic plasma simulation. VORPAL includes a cut cell algorithm to model complex boundaries, surface models for secondary electrons, and Monte Carlo models for ionization. Because VORPAL can scale well to large numbers of processors, one can model particularly difficult problems that are otherwise intractable. The geometric configuration of

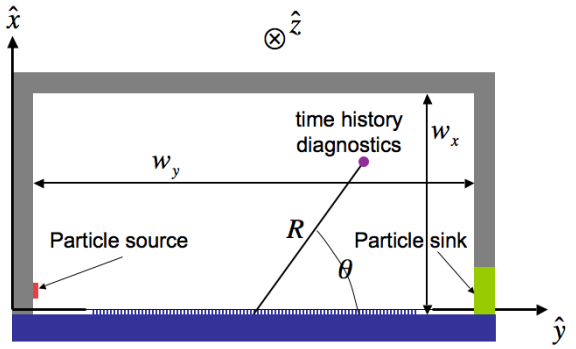


Figure 1: Schematics of the SPFEL geometry used in VORPAL. The 2D (3D) computational domain has size $w_x \times w_y$ ( $w_x \times w_y \times w_z$). History diagnostics are located at various angle ($\theta$) above the grating.

our simulation model is shown in Fig. 1. The model includes a rectangular perfectly-conducting grating, a particle source (on the left end side) and a particle "sink" on the right. The grating groves are along the $\hat{z}$ direction and the beam propagated along the $\hat{y}$ axis. Beside the grating, the other surrounding boundaries consist of perfectly matched layer (PML) that significantly suppresses artificial reflections of incident radiation.

The electric and magnetic fields histories are recorded at various locations far from the grating to provide information on the radiation spatial distribution. The particle source produces a uniformly-distributed (in all directions) DC beam with RMS transverse sizes $\sigma_{x,y}$ and uncorrelated velocity spreads $\sigma_{vx,vy,vz}$ can be included. Finally the beam is transversely confined by applying a uniform external axial magnetic field $\mathbf{B} = B_e\hat{y}$.

The SPFEL mechanism operates in a manner similar to a high-gain amplifier: as the beam propagates above the grating the electromagnetic fields associated (both associated to the evanescent and radiative fields) grow as

$$\{E, B\}(t) = \{E_0, B_0\} \exp(t/\tau), \tag{1}$$

where $\tau^{-1}$ is the growth rate. The FEL process eventually saturates and the field amplitudes become constant, i.e. $\{E, B\}(t \to \infty) = \{E_\infty, B_\infty\}$. In the following we define the gain as $\mathcal{G} \equiv E_\infty/E_0$. In the numerical investigation of the SPFEL performed so far, both the electron source and grating are immersed in an axial magnetic field with typical magnitudes in the Tesla range. The field strongly guides the particles motion [10, 11] and without it the requirements on beam transverse emittances could be extremely challenging to drive a THz SPFEL operating in the BWO regime [12].

## BENCHMARKING WITH PREVIOUS WORK IN GHZ REGIME

In an attempt to benchmark our model with previous work, we considered an SPFEL configuration identical to the one described in Ref. [13] (see the parameter list compiled in Table 1 on page 3 of Ref. [13]) except for the current 20 A/m. Our results offers the same fundamental behavior as the ones reported in Ref. [13], with the fundamental frequency of the bunching occurring at $f = 4.55$ GHz, comparing to their MAGIC simulation's result of $f = 4.57$ GHz. A snapshot of the pertinent electromagnetic field components is shown in Fig. 2 and the $B_z$-field history recorded at $\theta = 82°$ is shown in Fig. 3 (blue trace in plot a) along with its FFT [Fig. 3 (b)].

In addition, we performed a set of 3D simulations. For these simulations the beam full width in the $\hat{z}$-direction was set to 10 cm and the current to 20 A, which retains the same current density as the compared 2D simulations. Overall the 3D simulations reproduce all the main features observed in the 2D simulations. In the 2D simulations, the strength of the evanescent fields was shown to influence the speed of bunching as a function of height above the grating. This feature is also observed in 3D, where the evanescent fields are strongest towards the center of a flat beam. In addition the 3D simulation shows a similar effect in the direction parallel to the grating grove, with the bunching near the edges of the beam forming latter from that near the center. A comparison of the FFT for the $B_z$ history recorded at $\theta = 82°$ is presented in Fig. 3. The dominant frequencies

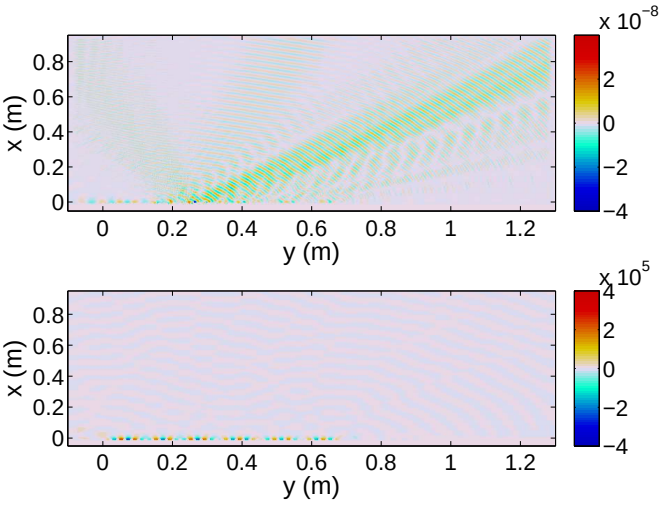


Figure 2: Snapshot of the electromagnetic fields $B_x(x, y)$ (top) and $E_y(x, y)$ (bottom) on the 2D simulation domain $(x, y)$ a time $t = 299$ ns. The strong E-fields associated to the evanescent wave can clearly been seen by inspection of the bottom plot (in the vicinity of $x = 0$).

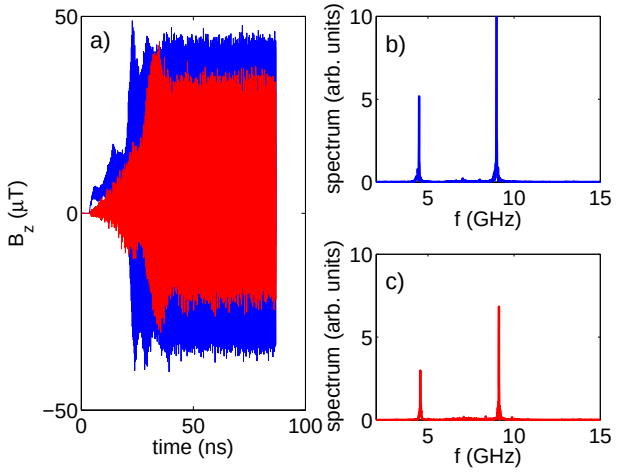


Figure 3: Comparison of the $B_z$ field history (a) and corresponding FFTs for 2D (b)and 3D (c) simulations in the GHz regime. The fundamental behaviors and frequency are roughly the same, with 4.397 GHz and 8.878 GHz for the 2D simulation, and 4.755 GHz and 8.952 GHz for the 3D simulation. In both cases, the 2nd harmonic is dominant, while the 2D simulation has greater magnitudes owing to the more discrete bunching.

are in good agreement, while the radiation is more prominent at those two frequencies in the 2D case due to its more discrete bunches. The amplitude of the magnetic field is weakened in the 3D case.

## TWO-DIMENSIONAL SIMULATIONS IN THE THZ REGIME

As a starting point for our simulations in the THz regime, we scaled down the GHz model described in the previous section by two order of magnitudes. The nominal parameters used for the THz simulations are presented in Tab. 1. The dimensions of the grating were kept the same for all the simulations presented henceforth while the beam parameters and external magnetic field were varied in an attempt to optimize the performance of the SPFEL process or investigate its sensitivity.

| parameter | value | units |
|---|---|---|
| Beam energy $\mathcal{E}$ | 50 | KeV |
| Current density $I$ | $[50-200]$ | A/m |
| Transverse emittance (rms) $\varepsilon_{x,y}$ | [0-0.5] | $\mu$m |
| Momentum spread (rms) $\sigma_\delta$ | [0-10] | % |
| External focusing $B_e$-field | [0.25-1] | T |
| Grating period | 200 | $\mu$m |
| Grove width | 100 | $\mu$m |
| Grove depth | 300 | $\mu$m |

Table 1: Parameters used for the simulations of the THz SPFEL.

The results from 2D simulations showed the same fundamental process as for the GHz scale, with a backward moving evanescent wave causing increasing bunching for sufficiently high current densities. We also found collective effects, most probably image charge, significantly affect the beam dynamics. This is especially important as the beam gets micro-bunched by the evanescent wave giving rise to large local charge concentrations (the microbunches). Such deleterious effects require higher external magnetic field than calculated in Ref. [14] or propagating the beam at larger distances from the grating (which results in a lower growth rate due the exponential decay of the evanescent E-field [$E_x(x,y) = E_0(x)\exp(-\alpha y)$]. Figure 4 shows an example of observed transverse instability where as the beam is being bunched it is steered toward the grating despite the large value of the axial B-field field $B_e = 2$ T.

Figure 5 depicts the results associated to a THz simulation with parameters gathered Tab. 1. For this set of simulation the current density was 50 A/m, $B_e = 1$ T, and the beam was 50 $\mu$m thick with its lower boundary located 25 $\mu$m above the grating groves. The field history [Fig. 5(a)], recorded a an observation angle $\theta = 76°$, clearly displays an exponential growth behavior [for $0.5 < t\,(\text{ns}) < 1.2$]. Several tests were performed with either uncorrelated longitudinal and transverse emittance spreads on the order of a few percent of the beam velocity. A 5% rms longitudinal velocity spread eliminate bunching for a beam similar to that used for Fig. 5. Simulation including transverse emittance show that an emittance of $\epsilon_x \simeq 0.2$ $\mu$m does not appreciably impact the performance

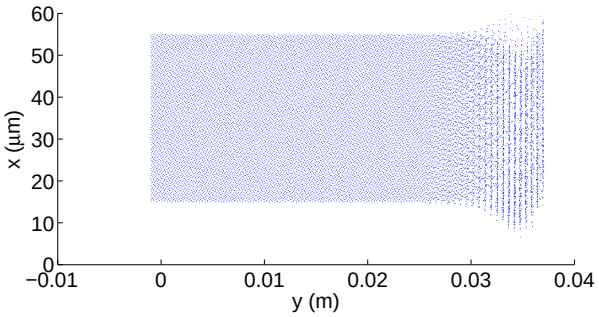


Figure 4: Example of "transverse instability" observed as the beam get bunched. Despite the large external axial field ($B_e = 2$ T) the beam is strongly steered toward the grating during the bunching process.

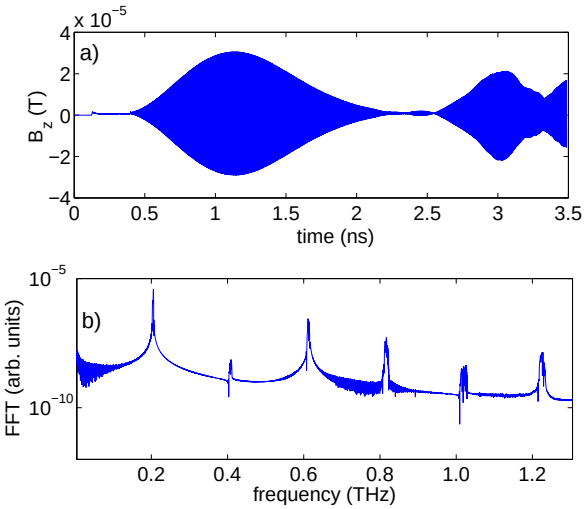


Figure 5: $B_z$-field history (a) and corresponding FFTs for 2D simulations in the THz regime. The first and third harmonic of the field occur at 0.2055 THz and 0.6111 THz.

of the SPFEL. Larger emittance values still produced significant bunching but also resulted in the beam to hit the grating (even with a strong magnetic field $B_e = 2$ T). The latter problem can obviously be mitigated by placing the beam farther from the grating at the expense of the strength of the interaction with the evanescent fields.

## IMPROVEMENT USING A PAIR OF PARALLEL GRATINGS

An additional grating placed above the original grating upside down is a straightforward way of enhancing the performance of the SPFEL. It will (1) increase the strength of the axial electric field responsible for the bunching and (2) produce a more uniform bunching across the height of the electron bunch. Such a grating was implemented in our model and preliminary simulations aimed at exploring the impact on bunching are shown in Fig. 6. For these simulations the gap between the two grating is 60 $\mu$m. As

anticipated the startup of SPFEL process is approximately twice as fast as the case of a single grating. Further analysis

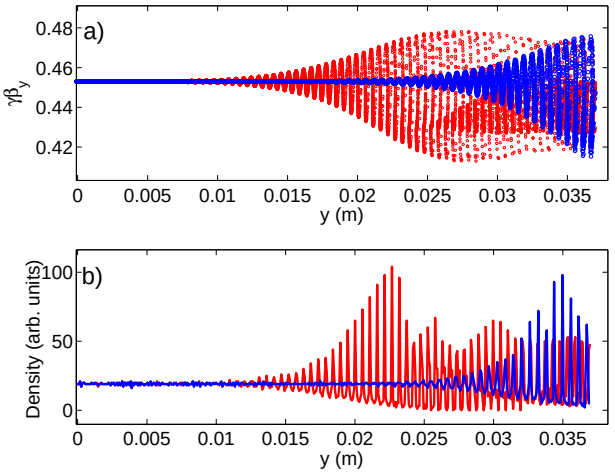


Figure 6: Snapshots at $t = 925$ ps of the $(y, \beta_y\gamma)$ phase space (a) and the corresponding current density (b) for two THz SPFEL configurations consisting of one (blue) or two (red) gratings.

of the phase space when color coded according to electron height further reveals the important behavior, as shown in Fig. 7. In the case of a single grating, the electrons nearer to the grating experience a more accentuated affect in phase space due to stronger interaction with the evanescent fields. With the pair of gratings, the evanescent field from the upper grating adds to produce a more uniform effect on the electrons, resulting in greater coherence if the beam is used with a secondary grating downstream to produce radiation.

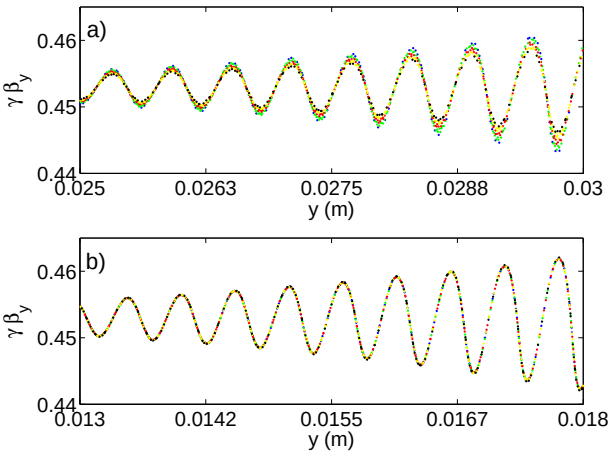


Figure 7: Zoomed snapshot of the axial phase space at $t = 925$ ps for the single- (a) and double- (b) grating configurations. The color coding corresponds to different beam slices in the $x$ direction: the beam at emission was divided into five radial slices of same thickness.

## SUMMARY

A free-electron laser based on the Smith-Purcell effect was successfully modeled at the GHz and THz regimes using VORPAL. The process is shown to have the same fundamental behavior in both 2D and 3D simulations. In particular, we used this model to explore a dual grating configuration and demonstrate it can more efficiently bunch the beam compared to the standard SPFEL configuration explored so far by other groups. The numerical model presented in this paper is currently being used in a start-to-end simulation of a complete table-top THz light source.

## ACKNOWLEDGMENTS

We are thankful to Dr. Vinit Kumar for fruitful discussions and for sharing his unpublished work with us. We are indebted to Dr. Panagiotis Spentzouris (Fermilab) for granting us access to the NERSC supercomputers. This work was partially supported by the US Department of Education under contract number P116Z050086 with Northern Illinois University.

## REFERENCES

[1] J. M. Wachtel, *J. Appl. Phys.*, **50** (1) (1979).

[2] H. L. Andrews and C. A. Brau, *Phys. Rev. ST-AB* **12**, 070701 (2004).

[3] V. Kumar and K.-J. Kim, *Phys. Rev.* **E 73**, 026501 (2006).

[4] L. Schaechter and A. Ron, *Phys. Rev.*, **A 40**, 876 (1989).

[5] K.-J. Kim, S.-B. Song, *Nucl. Instr. Meth.* **A 475**, 158 (2001).

[6] J. T. Donohue, J. Gardelle, these proceedings.

[7] H. L. Andrews, C. A. Brau, J. D. Jarvis, C. F. Guertin, A. O'Donnell, B. Durant, T. H. Lowell, M. R. Mross *Phys. Rev. ST-AB* **12**, 080703 (2009).

[8] N. Vinogradov, P. Piot, C. R. Prokop, J. W. Lewellen, and J. Noonan, Proceedings of LINAC08, Sept 29-Oct. 3, 2008, Victoria, BC, Canada, 554 (2008).

[9] C. Nieter and J. R. Cary, *J. Comp. Phys.*, **196**, 448 (2004); for current capabilities see webpage at http://www.txcorp.com/products/VORPAL/index.php

[10] J. T. Donohue, J. Gardelle, *Phys. Rev. ST-AB* **9**, 060701 (2006).

[11] D. Li, Z. Yang, K. Imasaki, and Gun-Sik Park, *Phys. Rev. ST Accel. Beams* **9**, 040701 (2006).

[12] K.-J. Kim and V. Kumar *Phys. Rev. ST-AB* **10**, 080702 (2007).

[13] J. T. Donohue, J. Gardelle, *Phys. Rev. ST-AB* **8**, 060702 (2005).

[14] V. Kumar and K.-J. Kim, *Phys. Rev. ST-AB* **12**, 070703 (2009).